metals

MDPI

Article

Surface Topography Measurement of Mirror-Finished Surfaces Using Fringe-Patterned Illumination

Shaowei Fu [1,2], Fang Cheng [1,*] and Tegoeh Tjahjowidodo [3]

[1] Advanced Remanufacturing and Technology Centre (Agency for Science, Technology and Research), Singapore 637143, Singapore; fu_shaowei@artc.a-star.edu.sg
[2] JM Vistec System Pte Ltd., Singapore 415938, Singapore
[3] Department of Mechanical Engineering, Katholieke Universiteit Leuven, 3001 Leuven, Belgium; tegoeh.tjahjowidodo@kuleuven.be
* Correspondence: chengf@artc.a-star.edu.sg; Tel.: +65-8125-7159

Received: 27 November 2019; Accepted: 19 December 2019; Published: 1 January 2020

Abstract: Mirror-finished surface products have a wide range of applications in different engineering industries, such as power generation, aerospace, semiconductors and optics. The surface topography of mirror-finished products is typically measured in a metrology laboratory, which is typically time consuming and cannot be integrated into the manufacturing process. To allow for in-situ product quality assurance and automatic tool change for manufacturing processes, a more accurate and responsive surface-measurement method is needed. For highly polished surfaces, a sub-micron surface fluctuation makes it possible to use light-scattering effects and image processing for surface texture analysis. A non-contact surface inspection system using a fringe-patterned illumination method is proposed in this paper. A predesigned pattern was projected onto the target surface, and its reflected image was captured by a camera. It was found that the surface parameters *Sa* and *Sq*, which are widely used to evaluate surface quality, are significantly correlated with luminous-intensity distribution. Another parameter, *Str*, which quantifies the uniformity of surface-texture directions due to polishing or grinding marks, was traditionally quantified after a complete-surface topographic measurement. In this research, a new approach is proposed to determine surface isotropy through a luminance-intensity distribution analysis. By rotating the test coupon, the variation of specular reflection showed correlation with the significance of surface-texture direction. The experimental results demonstrate that mirror-finished surfaces with a large deviation in luminance intensity across the pattern possess low *Str* values, which indicates low uniformity in surface texture.

Keywords: in-situ inspection; luminance contrast; fringe-patterned illumination; surface topography

1. Introduction

In the American Society for Testing and Materials (ASTM) standard A480 [1], the surface finish of stainless steel is defined by eight grades. The highest grade, i.e., mirror finish, is defined as a super-smooth finish usually manufactured through a polishing process with finer-grit abrasives and ending with buff polishing. In recent years, mirror-finished surface products have been applied extensively in many engineering industries. The aerospace industry has a strong demand for high finish quality in aircrafts' leading edges to help to reduce drag (air resistance) in flight [2]. In the optical industry, prism arrays [3], polygon mirrors [4], and projection lenses of optical lithography [5], which are key parts of advanced machines or optical instruments, need to be fabricated with a high quality of surface finishing. Semiconductor wafers, basic components used in integrated-circuit (IC) fabrication,

are required to be mirror-polished to improve IC chip performance [6]. In the medical industry, orthopaedic implants such as knee or hip prostheses need to be polished to a mirror finish to reduce friction and increase their lifespan [7].

A mirror-finished surface can be achieved through different machining processes, such as chemical mechanical polishing [8], magnetorheological finishing [9], abrasive flow machining [10] and elastic emission machining [11]. In semiconductor manufacturing, chemical mechanical polishing or planarization has been the most widely used method of producing mirror-finished surfaces since the early 1990s. Polishing is usually conducted without allowing the fine abrasive particles to create brittle fractures on the workpiece surface, while subtracting these materials in minute steps to finally fabricate a mirror-finished surface [12].

According to different national standards [1,13], the quality of the mirror-finished surface is specified in only a qualitative way, e.g., "a non-directional finish that is reflective and has good image clarity". However, the industry needs to quantitatively differentiate the mirror-finished surfaces among diverse products. The mirror-finished surface topography is the most important surface geometry and physical property for mirror-finished components [14]. An in-situ surface-topography measurement system is crucial to reducing rejections and costs. The in-situ measurement system should be able to perform in-situ inspection and give feedback of the inspection results to the machine operator to determine the next process for the products.

Optical techniques show great advantages in measuring mirror-finished surfaces due to their nature of as a non-contact mechanism that will thus prevent damage and contamination during measurement [15]. Interferometers are widely used both in academy and industry for the surface characterization of mirror surfaces [16]. Extremely high measurement accuracy, down to a sub-nanometer, can be achieved with heterodyne or phase-modulation techniques [17]. However, most conventional interferometers are costly and are required to be operated in a controlled laboratory environment. Some research has been carried out to develop fast and in-situ methods to measure mirror-finished surfaces. El-Hayek et al. [18] developed an optical single-scanning probing system to measure and characterize the form of an aspheric lens. Fuh et al. [19] developed a system for in-process measurement of surface roughness by combining an optical probe and adaptive optics. Speckle metrology [20] has been verified and deployed to measure the surface roughness of bulk metallic glasses through a laser-scattering method with adaptive optics, and can be integrated into a manufacturing process for in-situ measurement [21]. Recently, Sugino et al. [22] proposed a patterned area illumination method to measure the specular reflection of the polished metal surfaces and study the correlation between the surface topography and glossiness values. This can be seen as a potential solution to perform non-contact and in-situ mirror-finished surface measurement.

In this paper, a non-contact surface inspection system using the fringe-patterned illumination method [23] was developed to address the need for topography measurement on mirror-finished surfaces. By analysing the luminance contrast of the fringe-patterned images, the experimental results show that the developed system can achieve in-situ surface-topography measurement. In addition, the developed fringe-patterned illumination method is also readily applicable to determine the effects of polishing marks on mirror-finished surfaces. Overall, the developed system could be a key enabler to achieve in-situ measurement in the areas of surface characterisation and product verification.

2. Materials and Methods

2.1. Test Coupons

For surface-topography measurement, sixteen test coupons made from stainless steel, as shown in Figure 1, were ground and polished using an EcoMet 300 Pro (BUEHLER, Lake Bluff, IL, USA). These sixteen test coupons had a range of surface roughness values which accurately represent the different surface conditions of fan blades and turbine blades which have been widely used in the aerospace and power generation industries.

Figure 1. Test coupons for surface roughness measurement.

2.2. Coherence Scanning Interferometer

According to ISO 25178-604 [24], coherence-scanning interferometry is a surface-topography-measurement technique whereby the interference fringe localization provides quantitative information to characterize the surface topography during scanning of the optical path length. It includes, but is not limited to, measuring instruments that use spectrally broadband visible sources (white light) to attain the localization of interference fringes.

A beam splitter in the optical system of the coherence scanning interferometer separates the light into two beams, one directed to the reference mirror and the other directed to the test surface. After combining the two reflected light beams, the interference fringes can be generated if the optical paths of the two beams are equal. The interference fringes can be sensed for each surface point correlated to each pixel of the imaging camera. By vertically scanning the interferometric objective lens using a piezoelectric actuator, a surface topography map can be determined by finding the best equal-path condition at each pixel in the imaging camera [25,26].

Conventionally, the coherence-scanning interferometer serves as a standard method to measure smooth surface topography [27,28]. In this study, the surface topography of the sixteen test coupons was measured using a coherence scanning interferometer with a 20× objective lens (Talysurf CCI HD, AMETEK, Berwyn, PA, USA) as shown in Figure 2a. The Talysurf CCI HD can provide a vertical resolution of 0.1 nm and a lateral resolution of 1 μm.

Each test coupon was repeatedly measured five times with a measurement area of 2 mm × 2 mm. As an illustration, Figure 2b shows the surface topography measurement results of four test coupons with different surface roughness values. After form removal by third-order polynomials, the arithmetical mean roughness *Sa*, root mean square roughness *Sq* and texture aspect ratio *Str* defined in ISO 25178-2 [29] can be computed using the TalyMap surface analysis software (Talysurf CCI HD, AMETEK, Berwyn, PA, USA). The *Sa* and *Sq* parameters are by far the most universally recognized and well used parameters for surface-topography measurement in both academia and industry. The *Str* parameter is the most suitable parameter used to characterise the uniformity of surface texture [30].

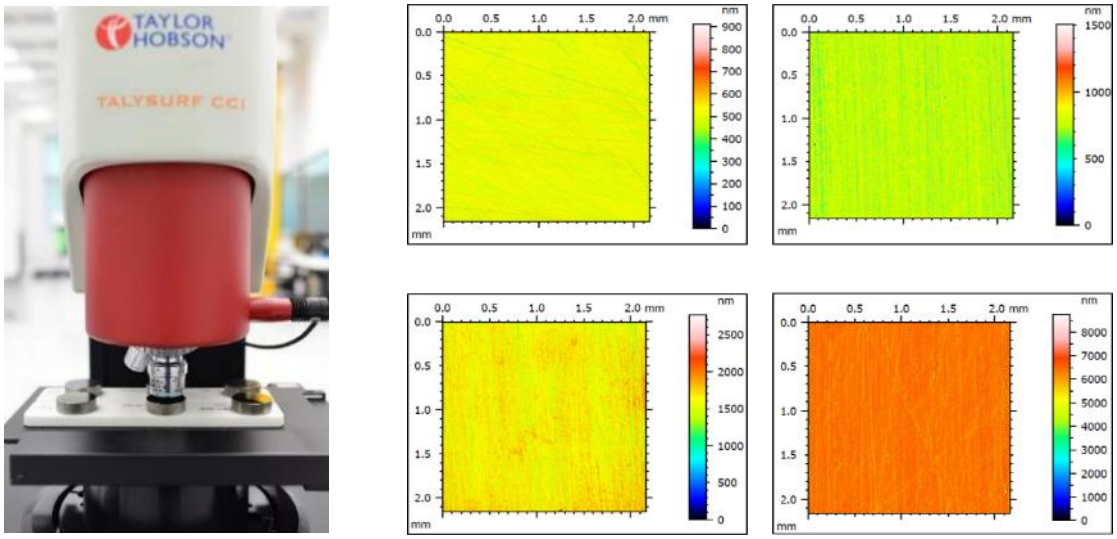

Figure 2. (**a**) Coherence scanning interferometer (Talysurf CCI HD); (**b**) Surface topography of test coupons.

2.3. Mirror-Finished Surface Measurement System

2.3.1. Modelling and Software Development

The key components of the developed mirror-finished surface-measurement system include a liquid crystal display (LCD) screen and an imaging device. Figure 3 shows the schematic illustration of the surface-measurement system. A fringe pattern of black-and-white stripes is generated by the LCD screen. In specular reflection, the reflection angle is equal to the incidence angle. Therefore, when the fringe patterns are projected on the mirror-finished surface, a mirror-like reflected image of the fringe patterns can be captured by the imaging device. The sharpness and contrast of the fringe patterns in the captured image can provide information associated with specular reflection on the surface and surface roughness level [22]. To analyse the sharpness and contrast of the fringe patterns, the image processing task includes fringe-pattern generation, pattern recognition, and fringe pattern analysis.

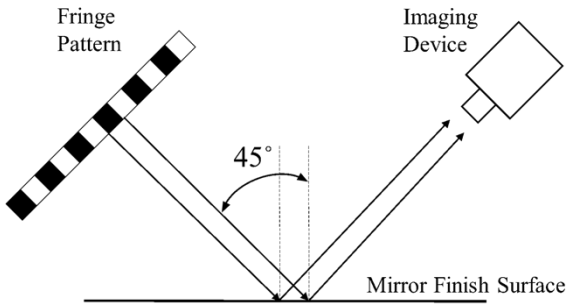

Figure 3. Schematic illustration of the surface-measurement system.

As an illustration, Figure 4 shows the black-and-white fringes projected on the surface of test coupons, and surface-topography plots measured using Talysurf CCI HD with different roughness levels. It can be clearly seen that from coupon 1 to coupon 4, the image of black-and-white fringes became blurred while surface roughness increased, as reflected by the surface-height scale bar. Subsequently, by referring to the sharpness of the black-and-white fringes and the surface roughness values measured using Talysurf CCI HD, a mathematical correlation can be determined.

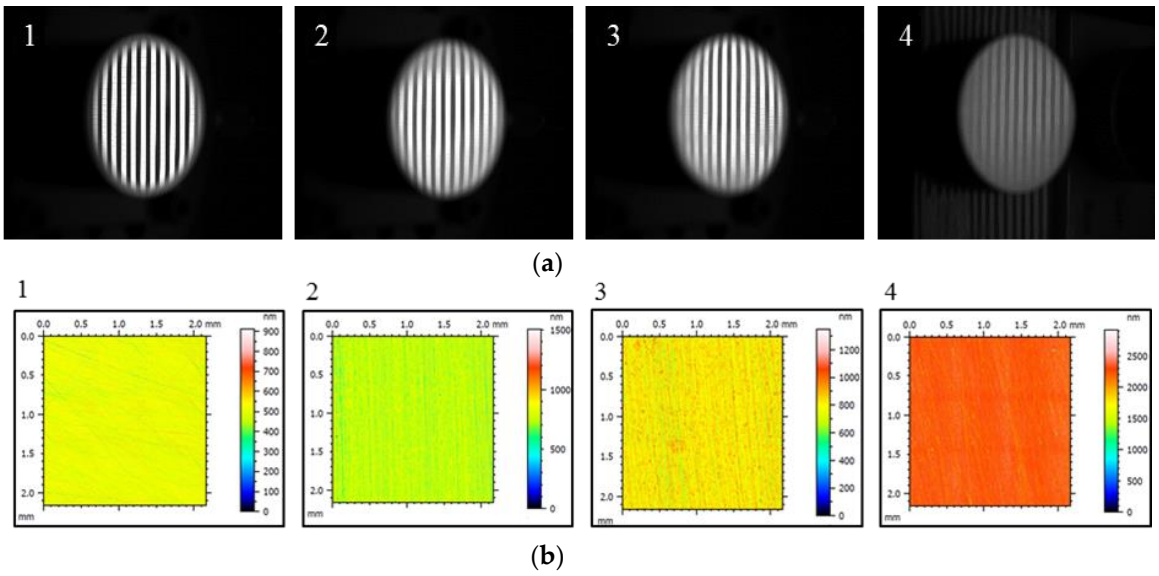

Figure 4. (**a**) Fringe pattern image captured by machine vision camera; (**b**) surface topography of test coupons measured by using Talysurf CCI HD.

Luminance contrast has been widely used to quantify image sharpness [31]. It is a measure of the perceived lightness or brightness difference between two colours [32]. The Michelson contrast is one of the luminance contrast definitions which is commonly used for simple periodic patterns where both bright and dark features take up similar fractions of the image area (e.g., sinusoidal gratings) [33]. The Michelson contrast is defined as

$$C_M = \frac{L_{max} - L_{min}}{L_{max} + L_{min}} \quad (1)$$

where L_{max} and L_{min} are the maximum- and minimum-luminance in the image, respectively. However, the Michelson contrast is usually influenced by the image noise and the variations of surrounding illumination. In order to reduce the image-noise level, the Michelson contrast C_M was modified in the developed imaging-processing algorithm as

$$C = \frac{AW - AB}{AW + AB} \quad (2)$$

where AW and AB are the arithmetic mean of the luminance intensity in the white fringes and black fringes, respectively.

The developed software program consists of an image-acquisition part and an image-processing part. The LabVIEW vision development module (National Instruments, Austin, TX, USA) was chosen to conduct the software program development to achieve in-situ inspection. The LabVIEW vision development module has a widely applicable library to integrate different types of machine-vision cameras. The image-acquisition part of the software program was completed using the IMAQ function inside the vision-development library. Additionally, the machine-vision camera can be controlled using a computer, and the captured image can subsequently be post-processed. The image-processing procedures for surface roughness measurements are listed below.

1. Create the region of interest on the acquired image.
2. Extract the intensity plane of the image to get the grayscale image.
3. Dilate the grayscale image to increase contrast and sharpness.
4. Use a median filter to remove the background noises.
5. Locate the measurement areas and calculate the average intensity of the black and white fringes.
6. Calculate the contrast and surface roughness based on the proposed empirical equations.
7. Display the contrast and roughness-measurement results in the inspection front window.

Figure 5 shows a preliminary image-process result for the surface roughness measurement of a test coupon. It can be observed that the image's contrast and sharpness increased, and the background noise was reduced after image processing. The contrast and surface roughness calculated based on empirical equations can be displaced in the inspection front window.

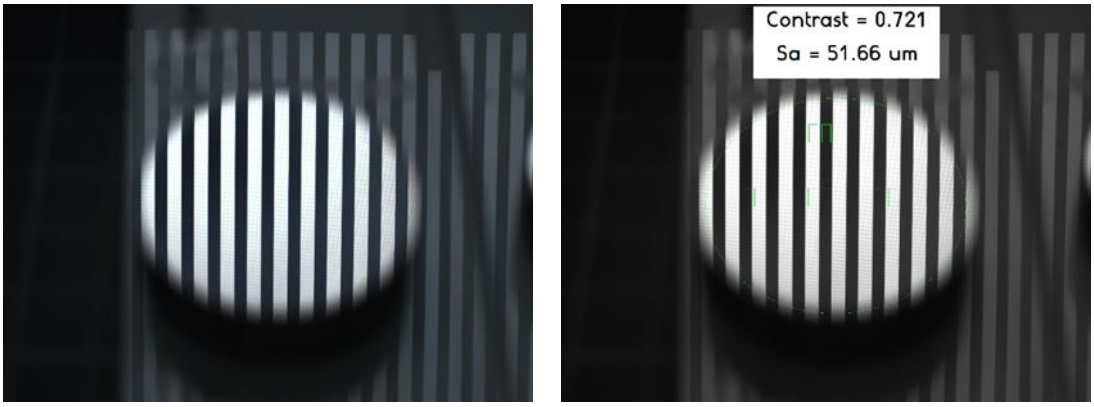

(**a**) (**b**)

Figure 5. Image processing for surface roughness measurement. (**a**) Original image; (**b**) result display.

2.3.2. Inspection System Setup

The developed inspection system includes two modules: a sensor module and an image-processing module. Figure 6 shows the configuration of the inspection system installed on an industrial robot (IRB 140, ABB, Zurich, Switzerland) to perform in-situ surface measurement. A computer-generated fringe pattern was displayed by an LCD screen (iPad Mini 3, Apple Inc., Cupertino, CA, USA). Reflected by the mirror-finished surface, the image of the fringe patterns was captured by the monochrome industrial camera (TXG50, Baumer, Frauenfeld, Switzerland) and ultra-machine vision lens (M1620-MPW2, Computar, Cary, NC, USA). By analysing the luminance-contrast values (*C*) of the fringe patterns in the image, the surface roughness values could be quantified. The monochrome industrial camera and LCD screen were angled at 45° from the horizon and the distance between the camera and the workpiece was set to 0.1 m.

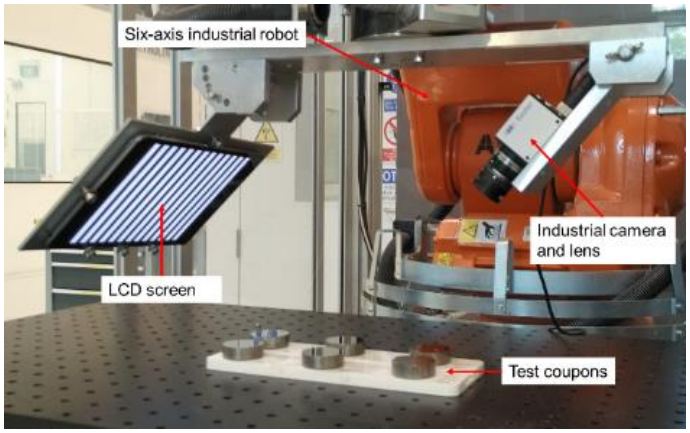

Figure 6. Robotic system setup for mirror-finished surface inspection.

3. Results and Discussion

As discussed in Section 2.1, sixteen test coupons with different surface roughness values were prepared in the experiments. The coupon size was 30 mm in diameter, and each coupon was measured in five areas, as illustrated in Figure 7. The surface roughness parameters *Sa* and *Sq* were measured using the Talysurf CCI HD, where each measurement area was 2 mm by 2 mm. The surface roughness measurement results (mean ± st. dev) of the sixteen test coupons are presented in Figure

8. It can be observed that the sixteen test coupons have different *Sa* and *Sq* values in the range of 15 nm to 120 nm and 30 nm to 160 nm, respectively.

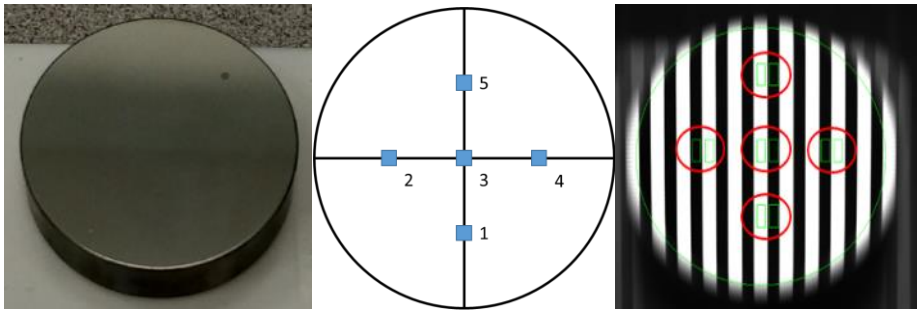

Figure 7. Measured areas on the coupon surface.

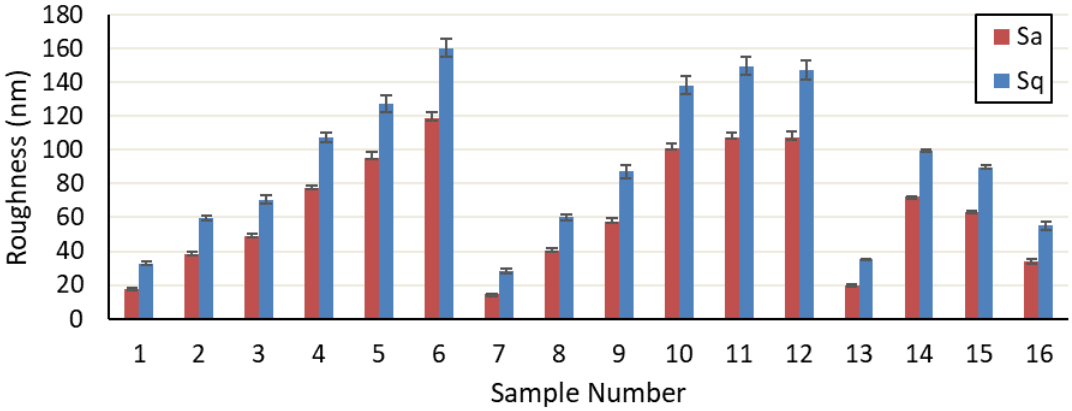

Figure 8. Roughness-measurement result using Talysurf CCI HD.

3.1. Luminance Contrast Measurement

The luminance contrast (*C*) measurement results (mean ± st. dev) of the sixteen test coupons are shown in Figure 9. The luminance contrast (*C*) measured by the fringe-patterned illumination system and the surface roughness parameters (*Sa* and *Sq*) measured by Talysurf CCI HD are presented as a correlation curve in Figures 10 and 11.

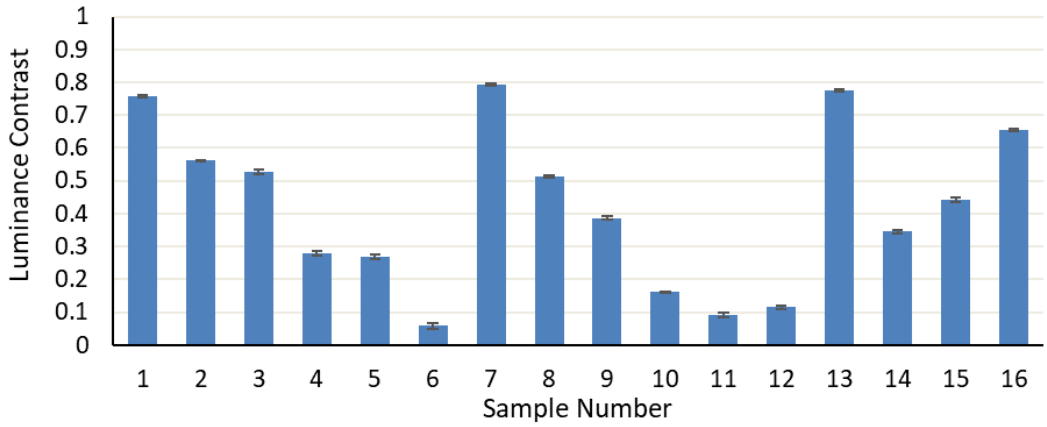

Figure 9. Luminance contrast measurement results.

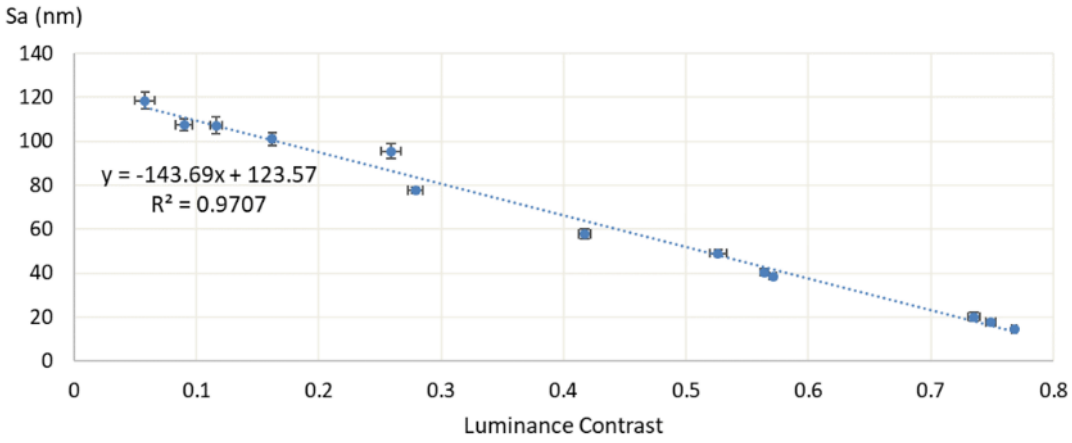

Figure 10. *Sa*-contrast curve.

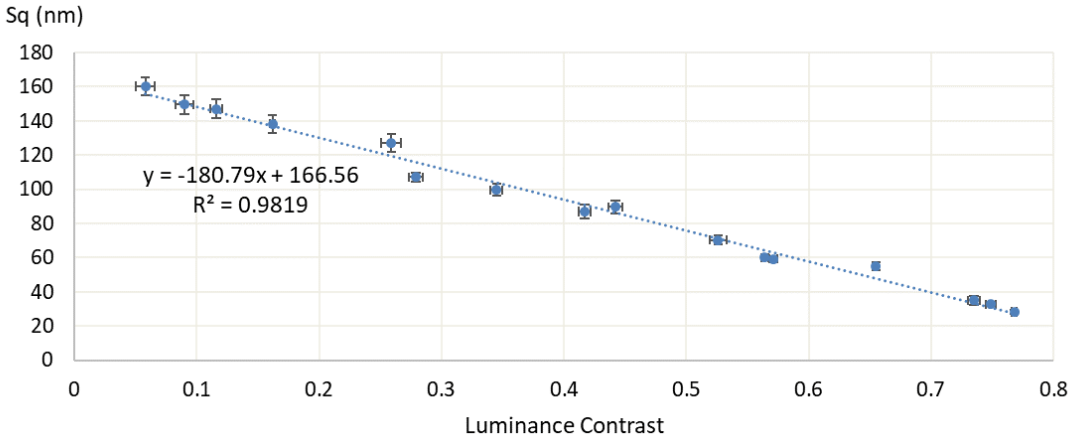

Figure 11. *Sq*-contrast curve.

The *Sa*-contrast curve in Figure 10 and the *Sq*-contrast curve in Figure 11 show the good capability of the fringe-patterned illumination system for the surface roughness measurement of the sixteen test coupons. As is well known and generally accepted, the coefficient of determination (R^2) determines how well the measured data points agree with the regression line. The closer the R^2 value is to one, the better the linear relationship between the two sets of data points. The high R^2 value of 0.9707 in the *Sa*-contrast curve and the value of 0.9819 in the *Sq*-contrast curve suggest that the data set can be regressed linearly.

From the surface roughness parameters (*Sa* and *Sq*) and luminance contrast (*C*) in Figures 10 and 11, the linear-regression models are represented by Equations (3) and (4). These two empirical-modelling equations are based on the preliminary measurement results of the sixteen test coupons. More test coupons need to be fabricated to add more measurement data in order to validate the empirical modelling equations.

$$S_a = -143.69C + 123.57 \quad (3)$$

$$S_q = -180.79C + 166.56 \quad (4)$$

3.2. Surface Uniformity Measurement

As stated by ISO 25178-2 [29], the texture aspect ratio parameter, *Str*, is a measure of the surface uniformity or directionality of the surface texture. The *Str* parameter has no unit and takes a value between 0 and 1. A surface with uniform texture will have an *Str* close to 1, while a surface with strong directional patterns will have an *Str* close to 0.

Coupon 2 and Coupon 8 were selected to evaluate the effects of polishing marks on the mirror-finished-surface uniformity. Figure 12 shows the microscopic images of the two test coupons. It can be clearly seen that the two test coupons represent two typical mirror-finished surfaces with unidirectional polishing marks and multi-directional polishing marks. As shown in Table 1, the two test coupons have very close *Sa* and *Sq* values, but the *Str* values of both test coupons indicate significant deviations.

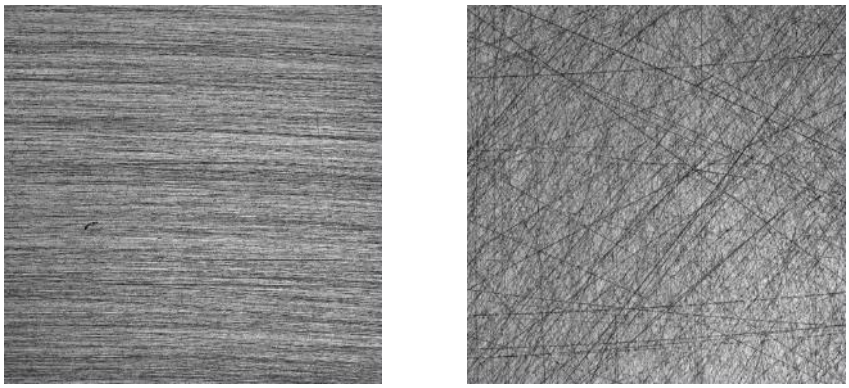

(**a**) (**b**)

Figure 12. Polishing marks on (**a**) Coupon 2; (**b**) Coupon 8.

Table 1. Measured surface roughness parameters of Coupon 2 and Coupon 8.

Coupon No.	*Sa* (nm)	*Sq* (nm)	*Str*
Coupon 2	38.6 ± 1.0	59.4 ± 1.5	0.072 ± 0.006
Coupon 8	40.4 ± 1.4	60.1 ± 1.8	0.426 ± 0.013

The luminance contrast values were measured using the image-processing algorithm described in Section 2.3.1. The measurement results at different measurement angles for Coupon 2 and Coupon 8 are plotted in Figure 13 to compare the difference of luminance contrast between them. For Coupon 2, the luminance contrast values at 0° and 180° are much larger than those at other measurement angles. In comparison, Coupon 8 demonstrates arbitrary and consistent luminance contrast values throughout all orientations.

In conclusion, the experimental result show that the luminance contrast value is correlated with the directions of the polishing marks and the fringe patterns at different measurement angles. The texture aspect ratio parameter *Str*, which characterises the surface uniformity, was experimentally studied and compared with the changes in luminance contrast.

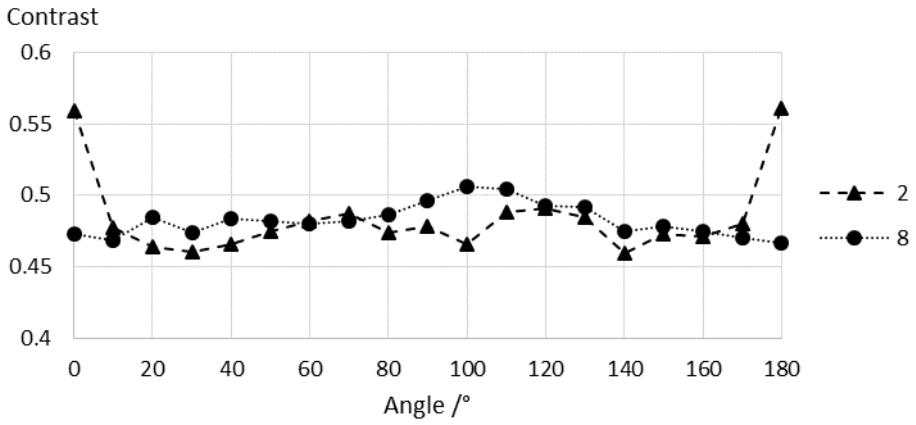

Figure 13. Luminance contrast values of different measurement angles.

4. Conclusions and Future Study

In this paper, a non-contact inspection system using the fringe-patterned illumination method was developed for in-situ topography measurement on mirror-finished surfaces. In the experimental study, the developed inspection system and a coherence scanning interferometer were used to measure the surface roughness of sixteen mirror-finished surface coupons. After comparing and analysing the experimental results, a reliable linear relation can be determined between surface roughness values and luminance contrast values. This demonstrates that the developed inspection system can be used to measure mirror-finished surfaces with *Sa* and *Sq* values in the ranges of 15 nm to 120 nm and 30 nm to 160 nm, respectively. Furthermore, the luminance contrast values at different measurement angles were able to determine the effects of polishing patterns on the mirror-finished surfaces. The texture aspect ratio parameter *Str*, which characterises the surface uniformity, was experimentally evaluated and compared with the changes in luminance contrast.

In future research, a new fringe pattern will be developed to evaluate the changes in two-directional luminance contrast and the texture aspect ratio parameter *Str* in 360-degree measurement. In addition, the effect of ambient illumination will be investigated and more mirror-finished test coupons will be manufactured to validate the fringe-patterned illumination method. Finally, optics simulation software will be used to evaluate the fringe-pattern illumination method for measuring non-flat mirror-finished surfaces.

Author Contributions: Conceptualization, S.F. and F.C.; methodology, S.F. and F.C.; software, S.F.; validation, S.F.; formal analysis, S.F. and F.C.; writing-original draft preparation, S.F.; Writing—review and editing, F.C. and T.T.; Supervision, F.C. and T.T. All authors have read and agreed to the published version of the manuscript.

Funding: This research was funded by Advanced Remanufacturing and Technology Centre (Singapore). The APC was funded by Advanced Remanufacturing and Technology Centre (Singapore).

Acknowledgments: The authors would like to thank Advanced Remanufacturing and Technology Centre (Singapore) for providing the experimental facility and materials. The authors would also like to thank Pooja Chaturvedi (Advanced Remanufacturing and Technology Centre, Singapore) for her support and contribution in language editing and proofreading.

Conflicts of Interest: The authors declare no conflict of interest. The funders had no role in the design of the study; in the collection, analyses, or interpretation of data; in the writing of the manuscript, and in the decision to publish the results.

References

1. ASTM. *A480/A480M 14b: Standard Specification for General Requirements for Flat-Rolled Stainless and Heat-Resisting Steel Plate, Sheet, and Strip*; ASTM International: West Conshohocken, PA, USA, 2014.
2. Bogue, R. Finishing robots: A review of technologies and applications. *Ind. Robot Int. J.* **2009**, *36*, 6–12.

3. Brinksmeier, E.; Riemer, O.; Gessenharter, A.; Autschbach, L. Polishing of Structured Molds. *CIRP Ann.-Manuf. Technol.* **2004**, *53*, 247–250.
4. Kanda, T.; Mitsuhashi, M.; Ueda, T.; Toyohara, A.; Yamamoto, K. New mirror-finish surface-grinding technology for the fabrication of optical device endfaces. In Proceedings of the International Conference on Optical Fabrication and Testing, Tokyo, Japan, 2 August 1995; Kasai, T., Ed.; International Society for Optics and Photonics: San Diego, CA, USA, 1995; Volume 2576, pp. 84–91.
5. Ando, M.; Negishi, M.; Takimoto, M.; Deguchi, A.; Nakamura, N. Super-smooth polishing on aspherical surfaces. *Nanotechnology* **1995**, *6*, 111–120.
6. Tay, C.; Wang, S.; Quan, C.; Ng, B.; Chan, K. Surface roughness investigation of semi-conductor wafers. *Opt. Laser Technol.* **2004**, *36*, 535–539.
7. Tournier, C.; Iabassene, C.; Guiot, A.; Quinsat, Y.; Of, G. Grinding of medical implants in cobalt-chromium alloy. In Proceedings of the 1st International Conference on Design and Processes for Medical Devices; Brescia, Italy, May 2012; pp. 95–98.
8. Zantye, P.B.; Kumar, A.; Sikder, A.K. Chemical mechanical planarization for microelectronics applications. *Mater. Sci. Eng. R Rep.* **2004**, *45*, 89–220.
9. Pollicove, H.M.; Fess, E.M.; Schoen, J.M. Deterministic manufacturing processes for precision optical surfaces. In Proceedings of the Window and Dome Technologies VIII, Orlando, FL, USA, 21–25 April 2003; Tustison, R.W., Ed.; International Society for Optics and Photonics: San Diego, CA, USA, 2003; p. 90.
10. Zhong, Z.W. Recent Advances in Polishing of Advanced Materials. *Mater. Manuf. Process.* **2008**, *23*, 449–456.
11. Kanaoka, M.; Takino, H.; Nomura, K.; Mori, Y.; Mimura, H.; Yamauchi, K. Removal properties of low-thermal-expansion materials with rotating-sphere elastic emission machining. *Sci. Technol. Adv. Mater.* **2007**, *8*, 170–172.
12. Han, X.; Gan, Y.X. Analysis the complex interaction among flexible nanoparticles and materials surface in the mechanical polishing process. *Appl. Surf. Sci.* **2011**, *257*, 3363–3373.
13. British Standards Institution. *BS 1449-2 Steel Plate, Sheet and Strip. Specification for Stainless and Heat-Resisting Steel Plate, Sheet and Strip*; British Standards Institution: London, UK, 1983.
14. Golkar, E.; Prabuwono, A.; Patel, A. Real-Time Curvature Defect Detection on Outer Surfaces Using Best-Fit Polynomial Interpolation. *Sensors* **2012**, *12*, 14774–14791.
15. Fu, S.; Cheng, F.; Tjahjowidodo, T.; Zhou, Y.; Butler, D. A Non-Contact Measuring System for In-Situ Surface Characterization Based on Laser Confocal Microscopy. *Sensors* **2018**, *18*, 2657.
16. Xue, S.; Chen, S.; Fan, Z.; Zhai, D. Adaptive wavefront interferometry for unknown free-form surfaces. *Opt. Express* **2018**, *26*, 21910–21928.
17. Yang, S.; Zhang, G. A review of interferometry for geometric measurement. *Meas. Sci. Technol.* **2018**, *29*, 102001.
18. El-Hayek, N.; Anwer, N.; Nouira, H.; Gibaru, O.; Damak, M.; Bourdet, P. 3D Measurement and Characterization of Ultra-precision Aspheric Surfaces. *Procedia CIRP* **2015**, *27*, 41–46.
19. Fuh, Y.K.; Wang, C.H. Adaptive Optics Integrated Surface Roughness Measurement of Sputtered PT Film on Silicon Substrate. *Microw. Opt. Technol. Lett.* **2013**, *55*, 2055–2059.
20. Joenathan, C.; Sirohi, R.S.; Bernal, A. Advances in Speckle Metrology. In *The Optics Encyclopedia: Basic Foundations and Practical Applications*; Wiley-VCH Verlag GmbH & Co. KGaA: Weinheim, Germany, 2015; pp. 1–99, ISBN 9783527600441.
21. Fuh, Y.-K.; Fan, J.R.; Huang, C.Y.; Jang, S.C. In-process surface roughness measurement of bulk metallic glass using an adaptive optics system for aberration correction. *Measurement* **2013**, *46*, 4200–4205.
22. Sugino, T.; Tashiro, Y.; Yamane, Y. Gloss Evaluation of Hairline-Finished Metal Surface Using Patterned Area Illumination Method: Relationship between Gloss Evaluation and Surface Roughness for the Estimation of Surface Roughness. *Key Eng. Mater.* **2017**, *749*, 251–256.
23. Fu, S.; Cheng, F.; Tjahjowidodo, T. Surface Texture Evaluation on Mirror Finish Surface Using Patterned Area Illumination Method. In *Lecture Notes in Mechanical Engineering*; Itoh, S., Shukla, S., Eds.; Springer: Singapore, 2020; pp. 155–162.
24. British Standards Institution. *BS EN ISO 25178-604-2013 Coherence Scanning Interferometry*; British Standards Institution: London, UK, 2013.
25. Vorburger, T.V.; Rhee, H.G.; Renegar, T.B.; Song, J.F.; Zheng, A. Comparison of optical and stylus methods for measurement of surface texture. *Int. J. Adv. Manuf. Technol.* **2007**, *33*, 110–118.

26. Lehmann, P.; Tereschenko, S.; Xie, W. Fundamental aspects of resolution and precision in vertical scanning white-light interferometry. *Surf. Topogr. Metrol. Prop.* **2016**, *4*, 024004.
27. de Groot, P. Coherence Scanning Interferometry. In *Optical Measurement of Surface Topography*; Springer: Berlin/Heidelberg, Germany, 2011; pp. 187–208.
28. Leach, R.; Leigh Brown, X.J.; Blunt, R.; Mike Conroy, D.M. *Guide for the Measurement of Smooth Surface Topography Using Coherence Scanning Interferometry*; National Physical Laboratory: London, UK, 2008.
29. British Standards Institution. *BS EN ISO 25178-2 Terms, Definitions and Surface Texture Parameters*; British Standards Institution: London, UK, 2012.
30. Leach, R. *Characterisation of Areal Surface Texture*; Springer: Berlin, Germany, 2013; ISBN 978-3-642-36457-0.
31. Pelli, D.G.; Bex, P. Measuring contrast sensitivity. *Vis. Res.* **2013**, *90*, 10–14.
32. Cowan, W.B.; MacIntyre, B. A practical approach to calculating luminance contrast on a CRT. *ACM Trans. Graph.* **1992**, *11*, 336–347.
33. Kukkonen, H.; Rovamo, J.; Tiippana, K.; Näsänen, R. Michelson contrast, RMS contrast and energy of various spatial stimuli at threshold. *Vis. Res.* **1993**, *33*, 1431–1436.